

Azimuthal Correlation Anisotropies in $p + p$ Collisions Simulated by Pythia

Manuel Sebastian Torres,^{1,2} Yicheng Feng,² and Fuqiang Wang²

¹*Department of Physics, Universidad Nacional de Colombia, Bogotá D.C. 111321, Colombia*

²*Department of Physics and Astronomy, Purdue University, West Lafayette, Indiana 47907, USA*

(Dated: October 18, 2024)

Stimulated by the keen interest of possible collective behavior in high-energy proton-proton and proton-nucleus collisions, we study two-particle angular correlations in pseudorapidity and azimuthal differences in simulated $p + p$ interactions by the Pythia 8 event generator. Multi-parton interactions and color connection are included in these simulations which have been perceived to produce collectivity in final-state particles. Meanwhile, contributions from genuine few-body nonflow correlations, not of collective flow behavior, are known to be severe in those small-system collisions. We present our Pythia correlation studies in a pedagogical way and report azimuthal harmonic anisotropies analyzed by several methods. We observe anisotropies in those Pythia simulated events qualitatively and semi-quantitatively similar to experimental data. Our findings highlight the delicate nature of azimuthal anisotropies in small-system collisions, and provide a benchmark helping improve data analysis and interpret experimental measurements in small-system collisions.

I. INTRODUCTION

One of the most interesting aspects of heavy ion collisions is the azimuthal angle distribution of particles in the final state. This is because the overlap geometry of the collision is anisotropic, like an almond shape. This anisotropic geometry is imprinted on the final state particle momentum distribution because of interactions among the particles before they freeze out [1]. Those interactions drive the collective expansion of the overlap collision system, a phenomenon called collective flow [2]. The comparison between the momentum anisotropy and the initial geometry anisotropy tells us information about the interactions in the hot and dense medium, the quark-gluon plasma (QGP), created in those collisions.

To study azimuthal anisotropies, particle distributions are often written in Fourier harmonic series in terms of the particle azimuthal angle (ϕ) relative to the reaction plane (Ψ) [3]:

$$\frac{dN}{d\phi} \propto 1 + \sum_{n=1}^{\infty} 2v_n \cos n(\phi - \Psi). \quad (1)$$

The coefficients, v_n , characterize the harmonic anisotropies. The most straightforward way to calculate the anisotropies is through two-particle correlations [4]:

$$\frac{dN}{d\Delta\phi} \propto 1 + \sum_{n=1}^{\infty} 2V_n \cos n\Delta\phi, \quad (2)$$

where $\Delta\phi = \phi_1 - \phi_2$ is the pair azimuthal opening angle. The Fourier coefficients, characterizing the two-particle cumulants, are given by

$$V_n = \langle \cos n\Delta\phi \rangle. \quad (3)$$

If the azimuthal anisotropy in $\Delta\phi$ comes all from global correlations of all particles with respect to the reaction plane (i.e. flow), then $v_n = \sqrt{V_n}$.

There are, however, two-particle correlations coming from processes like resonance decays and jets. These few-body correlations contribute to V_n , and are often referred to as nonflow [5–7], in contrast to the global flow correlations. Thus, V_n

contains both flow and nonflow contributions. Because nonflow arises from two- and few-body particle correlations, their effect is diluted by particle multiplicity, resulting in a typical inverse multiplicity dependence in the two-particle cumulants,

$$V_n = v_n^2 + C/N. \quad (4)$$

Because of the large multiplicity in mid-central and central heavy-ion collisions, nonflow contamination is minor compared to collective flow [8]. Nonflow can dominate in peripheral collisions where multiplicity is small.

In heavy ion collision studies, proton-proton ($p + p$) and proton-nucleus ($p + A$) collisions are often taken as references to infer properties of the QGP, or nuclear effects in hot QCD (quantum chromodynamics). It has long been considered that the particle azimuthal distributions in those small-system ($p + p$ and $p + A$) collisions should be uniform (there is no preferred azimuthal direction), and the two-particle anisotropy V_n in those small-system collisions must all be nonflow. However, recent experiments suggest that there may exist collective flow in $p + A$ and $p + p$ collisions, particularly in high-multiplicity events [9–21]; one strong indication is that the four- and multi-particle cumulants, essentially devoid of nonflow, are finite [22–24]. In two-particle cumulant measurements of Eq. (4), the nonflow effect can be severe because the event multiplicity, and thus the multiplicity dilution, is small. This is the case even in high-multiplicity events of those small-system collisions, where the multiplicity is comparable to that in peripheral heavy ion collisions. Many nonflow mitigation methods have been used [8, 25, 26]. After nonflow mitigation, it has been found in small system collisions, especially at LHC energies, that finite positive v_n^2 remain [26]. This led to the conclusion that a small QGP droplet may have been formed in small system collisions [26].

On the other hand, the overlap geometry in small-system collisions is lumpy due to fluctuations, and final-state momentum anisotropy could result if there is some degree of interactions [27–30], e.g., multi-parton interactions [31–34], in those small-system collisions. The magnitude of those interactions, gauged by the magnitude of the final-state momentum anisotropy relative to the initial geometry anisotropy, would

then discriminate whether the interactions happen in a low-density environment or a high-density QGP.

Besides those physics questions, the technical question of how well nonflow has been mitigated is not settled and is under extensive investigation. It is therefore interesting to examine anisotropies in model simulations of $p + p$ collisions, particularly by the Pythia event generator [35–38]. Pythia is naively not expected to generate single-particle azimuthal anisotropy because it is not a cascade model with final-state interactions. However, recent implementation of multi-parton interactions (color reconnection) is perceived to mimic some degree of final-state interactions, and thus it is not completely out of the question that there must be no collective flow [36, 39, 40]. Studies of anisotropies in Pythia would, therefore, be valuable in at least two fronts. One is to aid in studies of nonflow subtraction techniques and associated uncertainties [8, 41, 42], and the other is to discern any collective flow in $p + p$ interactions to guide the interpretations of experimental anisotropy measurements in small-system collisions [25, 26].

We hereby report a study of azimuthal correlation anisotropies in $p + p$ interactions simulated by Pythia version 8.303 [38], which includes multi-parton interactions and color reconnection [39, 40]. Our study may provide insights and perspective to help interpreting the apparent collective flow phenomenon observed in small-system collision experiments.

II. PYTHIA MODEL SETUP

We use Pythia 8.303 [38] to simulate $p + p$ collisions at the center-of-mass energy of $\sqrt{s_{NN}} = 200$ GeV. We generate 3×10^8 events each for diffractive and non-diffractive interactions with soft processes (SoftQCD) [36]. The soft processes in Pythia represent the entire cross-section (σ_{tot}) of the hadron-hadron interaction, i.e. minimum bias (MB) interaction. Rare processes, like jet physics at all scales, occur as part of the total cross-section. In the case of $p + p$ collision in Pythia, the cross section is calculated by the 1992 Donnachie-Landshoff parameterization [36]. This total cross-section is the sum of several components: $\sigma_{\text{tot}} = \sigma_{\text{sd}} + \sigma_{\text{dd}} + \sigma_{\text{nd}} + \sigma_{\text{el}}$ [43]. The diffractive part is divided into the single (sd) and the double (dd) component, where the former has the $pp \rightarrow pX$ processes while the latter has the $pp \rightarrow ppX$ processes. The diffractive events in our simulation include both single-diffractive and double-diffractive processes. The non-diffractive (nd) part includes all other inelastic processes $pp \rightarrow X$. The elastic (el) process, $pp \rightarrow pp$, does not produce particles and thus not included in our simulation. The comparison between diffractive and non-diffractive interactions is expected to shed lights onto initial- vs. final-state effects, because diffractive interactions should be more closely related to initial state of the proton whereas non-diffractive interactions could be influenced by final-state effects if any.

Table I lists the majority of particle species and their average compositions in non-diffractive events. In our simulations, we keep the electromagnetic- and weak-decay hadrons stable.

TABLE I. Average full-phase space multiplicities of various particle species in non-diffractive events generated by Pythia 8.303. A total of approximately 3×10^8 events are generated.

| particle multiplicity | | particle multiplicity | |
|-----------------------|--------|-----------------------|--------|
| π^+ | 12.140 | π^- | 11.422 |
| π^0 | 13.289 | | |
| K^+ | 1.631 | K^- | 1.459 |
| K^0 | 2.263 | \bar{K}^0 | 1.059 |
| p | 4.162 | \bar{p} | 0.700 |
| n | 1.768 | \bar{n} | 0.699 |
| Λ | 0.370 | $\bar{\Lambda}$ | 0.217 |

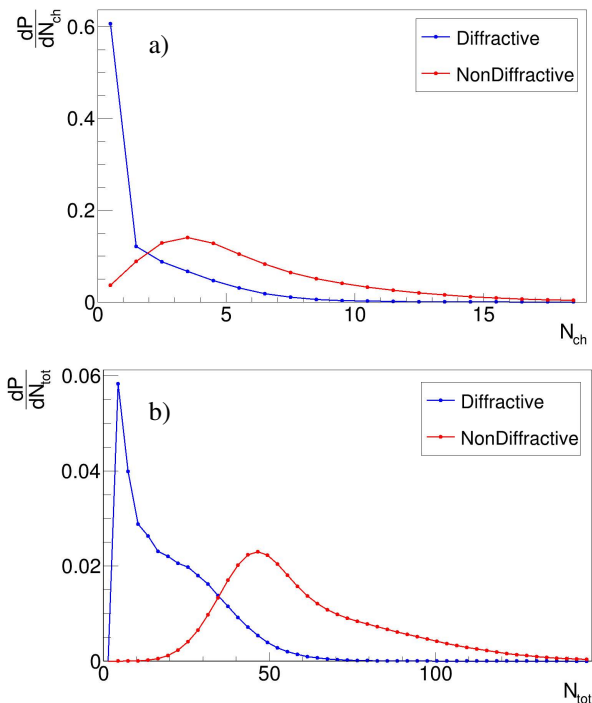


FIG. 1. Probability distributions of diffractive and non-diffractive $p + p$ collisions simulated by Pythia 8.303 as a function of (a) N_{ch} , the midrapidity (within $|\eta| < 1$ and $0.2 < p_{\perp} < 2$ GeV/c) charged hadron ($\pi^{\pm}, K^{\pm}, p, \bar{p}$) multiplicity, and (b) N_{tot} , the total final-state particle multiplicity (including all charged and neutral particles, over 4π solid angle).

We examine final-state particles (`status > 0` in Pythia). Since experiments (such as STAR [44] at RHIC and ALICE [45] at the LHC) usually measure charged particles in the limited midrapidity region, we will focus on charged hadrons within pseudorapidity range $|\eta| < 1$ and transverse momentum range $0.2 < p_{\perp} < 2$ GeV/c. Specifically, we include only $\pi^{\pm}, K^{\pm}, p, \bar{p}$ in our study, referred to as particles of interest (POI). Figure 1(a) shows the diffractive and non-diffractive event probability distributions in POI multiplicity within $|\eta| < 1$ and $0.2 < p_{\perp} < 2$ GeV/c, referred to as N_{ch} hereinafter. As reference the distribution in the total number of final-state particles (N_{tot}), including both charged and neutral

particles over all phase space, is shown in Fig. 1(b). Diffractive events have fewer produced particles than non-diffractive events, as expected.

Events of differing N_{ch} are expected to have varying physics, particularly in non-diffractive events, influences of final-state effects such as multi-parton interactions and color reconnection on possibly collective behavior. We thus divide the events into the following N_{ch} bins: 1–3, 4–6, 7–10, 11–14, 15–20. We study anisotropies of POI in N_{ch} bins. We present our results as a function of the mean multiplicity $\langle N_{\text{ch}} \rangle$ of each N_{ch} bin.

III. CORRELATION ANALYSIS

A. Two-particle cumulant anisotropy

We first examine the Fourier coefficients of Eq. (3). Figure 2 shows $\sqrt{V_n}$ as a function of the total multiplicity N_{tot} for both diffractive and non-diffractive events. It is observed that $\sqrt{V_2}$ decreases with N_{tot} and appears to saturate at large N_{tot} . Motivated by Eq. (4), we fit the data by $\sqrt{p_0^2 + p_1/N_{\text{tot}}}$. The fitted p_0 parameter is non-zero for both diffractive and non-diffractive events, suggesting that both types of events may have flow-like global anisotropies. The magnitudes of the p_0 parameter are comparable between diffractive and non-diffractive events.

Note that the fit quality is not good, indicating that the simple relation in Eq. (4) may not hold. For example, the nonflow correlation strength such as jet correlations may increase faster than linearly in multiplicity which would result in a slower decrease of V_n than $1/N_{\text{tot}}$. The global flow-like correlation of the underlying event may also change with the event multiplicity so a constant p_0 parameter may not be adequate. It is clear that a more rigorous investigation is needed in order to identify the structure of $p + p$ events from Pythia simulations.

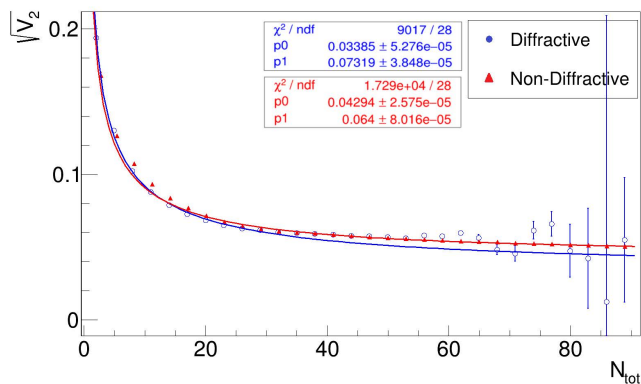


FIG. 2. Two-particle cumulant parameter, $\sqrt{V_2}$, as a function of the total multiplicity N_{tot} . Fit curves are $\sqrt{V_2} = \sqrt{p_0^2 + p_1/N_{\text{tot}}}$ where p_0 and p_1 are fit parameters.

B. Two-particle $(\Delta\eta, \Delta\phi)$ correlations

Two-particle $(\Delta\eta, \Delta\phi)$ correlations are widely used to identify sources of correlations, where $\Delta\eta \equiv \eta_1 - \eta_2$ and $\Delta\phi \equiv \phi_1 - \phi_2$ are the two-particle distances in pseudorapidity and azimuthal angle [46]. For example, resonance decays show up as a near-side peak at $(\Delta\eta, \Delta\phi) \approx (0, 0)$; so do intra-jet correlations. Effects of global momentum conservation and dijet correlations show up as away-side ridge peaked at $\Delta\phi = \pi$ and roughly uniform in $\Delta\eta$. Resonance decays and intra-jet correlations are hard to distinguish, so are global momentum conservation effect and dijet correlations. Global momentum conservation may be modeled by a negative $V_1 = \langle \cos \Delta\phi \rangle$ term [47], and others are often modeled by Gaussians. In our simulation of soft QCD interactions (i.e. MB events), jet contributions are minimal. However, high-multiplicity events are known to be biased towards stronger jet production [48].

Figure 3 shows $(\Delta\eta, \Delta\phi)$ correlations of POI from diffractive and non-diffractive events. The two-particle acceptance, approximately a triangle in $\Delta\eta$ as discussed below, has not been corrected in these plots. The shapes are similar between diffractive and non-diffractive events while the magnitude is significantly smaller in the former because of the smaller number of particles produced in diffractive events.

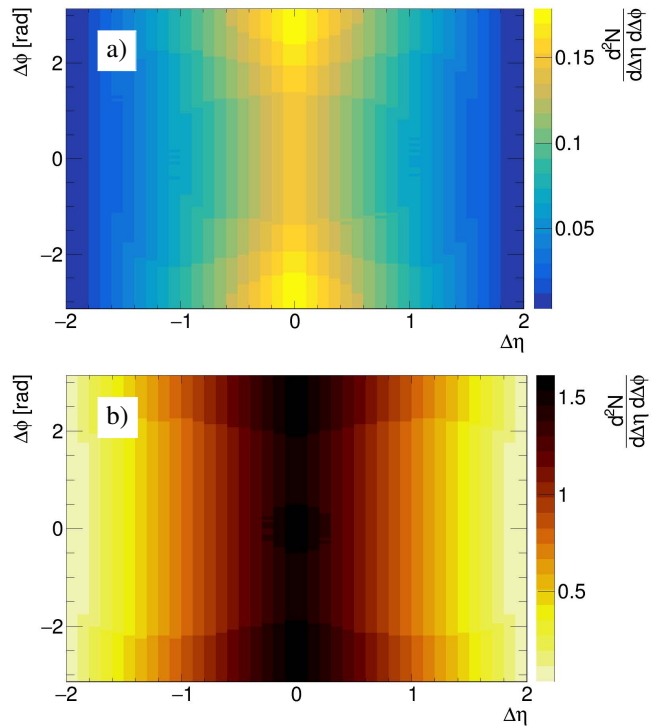


FIG. 3. Two-particle $(\Delta\eta, \Delta\phi)$ distributions from diffractive (a) and non-diffractive (b) interactions. The two-particle “triangle” acceptance in $\Delta\eta$ is not corrected. The z axis (color coordinate) is the number of pairs per unit of pseudorapidity per radian.

Before continuing, we want to correct for an important aspect, namely, the two-particle acceptance. This acceptance is approximately a triangle in $\Delta\eta$ and uniform in $\Delta\phi$, and

is often referred to as the “triangle” acceptance [49]. We obtain the two-particle acceptance factor by the mixed-event technique, taking one particle from one event and the other particle from another event of the *same multiplicity value* as the first event. The mixed-event correlations are obtained separately for diffractive events and non-diffractive events. The mixed-event correlation function is normalized such that the magnitude is unity at $\Delta\eta = 0$ because, with one particle within the η acceptance (in our case $|\eta| < 1$), the probability for the second particle to be inside the acceptance is 100% if $\Delta\eta = 0$. The normalized mixed-event correlation is divided to obtain the acceptance-corrected two-particle correlations.

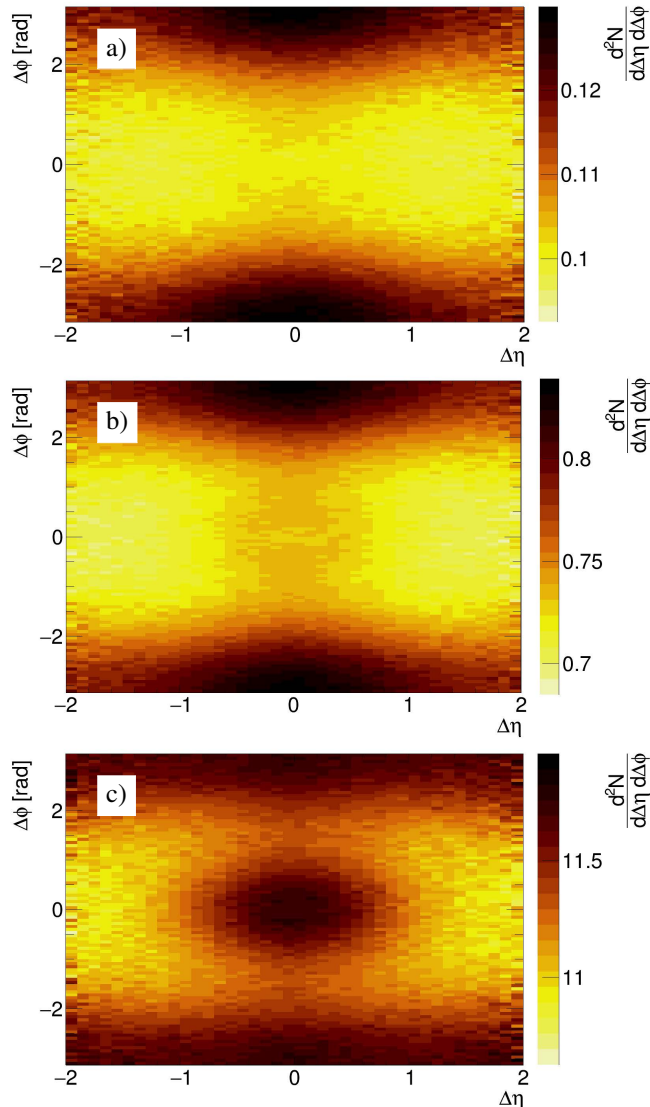


FIG. 4. Two-particle correlations in non-diffractive interactions, as in Fig. 3(b), in various multiplicity ranges of $1 \leq N_{\text{ch}} \leq 3$ (a), $4 \leq N_{\text{ch}} \leq 6$ (b), and $15 \leq N_{\text{ch}} \leq 20$ (c). The two-particle “triangle” acceptance in $\Delta\eta$ is corrected by mixed events of the corresponding multiplicity range. The z axis (color coordinate) is the number of pairs per unit of pseudorapidity per radian. For example, the $\Delta\eta$ -acceptance corrected total number of pairs is about 20 in panel b), giving an average amplitude of approximately 0.8.

Figure 4 shows the “triangle” acceptance corrected ($\Delta\eta, \Delta\phi$) correlations in non-diffractive interactions for three multiplicity ranges. The correlations feature a near-side peak ($\Delta\eta \approx 0, \Delta\phi \approx 0$) (most prominent in high multiplicity events) and a broad away-side ridge at $\Delta\phi \approx \pi$. These features are characteristic of intra-jet and inter-jet (dijet) correlations, as well as resonance decays and global momentum conservation. Correlations in diffractive interactions are similar. It is noteworthy that the near-side peak is not visible in low-multiplicity events, however, resonance decays (and similarly jet correlations) must be present in those events as well. As will be shown later, the negative V_1 component is large in those low-multiplicity events, such that the near-side correlation peak is submerged by the negative dip [14].

Far more resonances decay into daughters with a positive-negative charge pair than with a positive-positive or negative-negative charge pair. Intra-jet correlated hadrons have more opposite-charge pairs than same-charge pairs because jets are mostly neutral gluon jets (i.e., charge-ordering phenomenon in jets). One thus has stronger correlation in opposite-sign (OS) pairs than in same-sign (SS) pairs, and can learn more insights by analyzing OS and SS correlations separately.

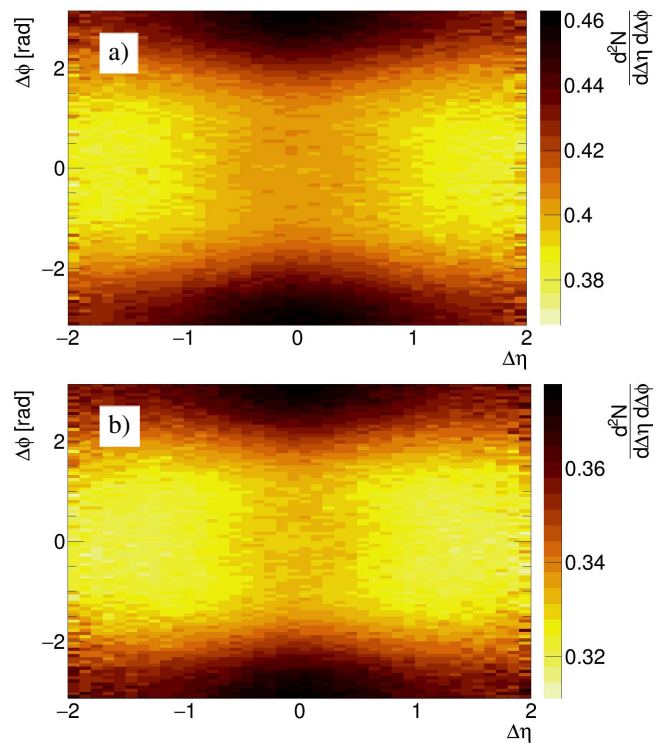


FIG. 5. Acceptance-corrected two-particle ($\Delta\eta, \Delta\phi$) correlations in non-diffractive collisions with $4 \leq N_{\text{ch}} \leq 6$ as in Fig. 4(b), but separately for OS pairs (a) and SS pairs (b). Correlations are similar in shapes for other multiplicity bins as well as for diffractive events.

Figure 5 shows the acceptance-corrected correlations, separately for OS and SS pairs, in non-diffractive $p + p$ collisions. One multiplicity bin is shown as an example; the results are similar in shape for other multiplicity bins. The near-side correlations are more prominent in OS correlations than in

SS correlations, reflecting resonance decays and charge ordering in (mini-)jet fragmentation. The away-side correlations ($\Delta\phi \approx \pi$) are similar between OS and SS correlations, indicating no charge-dependent correlations on the away side.

C. Charge-dependent correlations

Figure 6 shows the $\Delta\eta$ and $\Delta\phi$ projections of the OS and SS 2D correlation functions for non-diffractive events with $4 \leq N_{\text{ch}} \leq 6$ from Fig. 5. Other multiplicity bins are similar in the correlation shapes. The $\Delta\eta$ correlation is characteristic of a Gaussian centered at $\Delta\eta = 0$. The $\Delta\phi$ correlations are dominated by the away-side peak at $\Delta\phi = \pm\pi$, with little near-side peak at $\Delta\phi = 0$ visible at the scale of the plots because of the large negative dipole aforementioned.

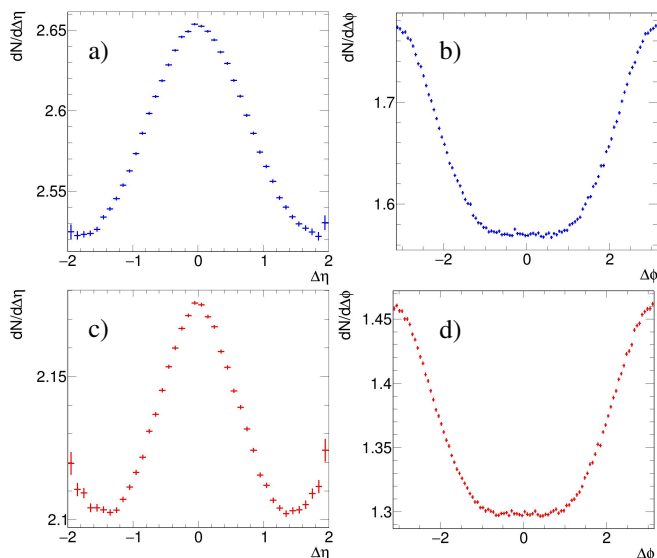


FIG. 6. Projections of the 2D correlation functions from Fig. 5 onto $\Delta\eta$ (a,c) and $\Delta\phi$ (b,d) for OS (a,b) and SS (c,d) pairs in non-diffractive events with $4 \leq N_{\text{ch}} \leq 6$. The correlations are normalized per event and by bin size.

The OS correlation contains more contributions from resonance decays and jets than the SS correlation. The number of OS and SS pairs from the underlying event also differ significantly as shown in Fig. 6. It requires careful analysis to study those charge-dependent nonflow correlations. We leave it to future work. In this work, we are interested in the possible flow-like anisotropies in $p + p$ events simulated by Pythia. Since the SS pairs are less contaminated by nonflow, we will focus on SS correlations.

D. Same-sign correlations

Although to a less degree than the OS pairs, SS pairs are affected by jet and dijet correlations as well. Intra-jet correlations are concentrated on the near side $\Delta\phi \sim 0$. The dijet correlations are back-to-back and concentrated on the

away side $\Delta\phi \sim \pm\pi$. Because the underlying parton-parton interaction kinematics are not necessarily symmetric about midrapidity, the away-side correlations are approximately $\Delta\eta$ independent. Other back-to-back correlations, such as global momentum conservation and possibly flow-like harmonics, are also mostly independent of $\Delta\eta$. One may thus take the difference between small- and large- $\Delta\eta$ correlations to assess the near-side nonflow correlations.

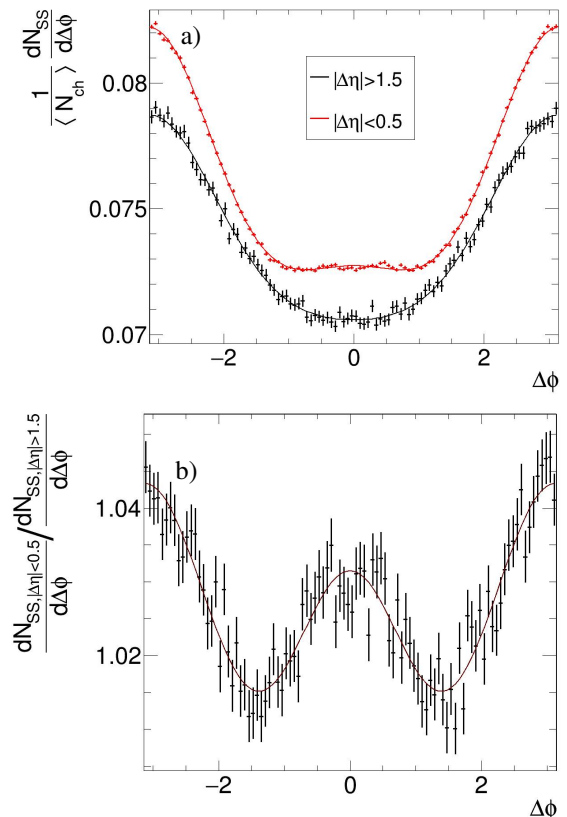


FIG. 7. (a) SS correlations in $\Delta\phi$ within small $|\Delta\eta| < 0.5$ and large $1.5 < |\Delta\eta| < 2$ for non-diffractive events with $4 \leq N_{\text{ch}} \leq 6$. The correlations are obtained from projections of the acceptance-corrected $(\Delta\eta, \Delta\phi)$ correlations in Fig. 5 in corresponding $\Delta\eta$ ranges, and are then divided by $\langle N_{\text{ch}} \rangle$ so they are SS dihadron correlations per hadron. Each superimposed curve is a fit to the corresponding data with the sum of a pedestal and two Gaussians, one centered at $\Delta\phi = 0$ and the other at $\Delta\phi = \pm\pi$. The fitted pedestals are 0.0708 ± 0.0007 and 0.0704 ± 0.0001 for small and large $\Delta\eta$, respectively. The central Gaussian amplitude for the large- $\Delta\eta$ correlation is negative. (b) Ratio of small- $\Delta\eta$ correlation over large- $\Delta\eta$ one. The superimposed curve is a fit to the same functional form as in panel a). The fitted pedestal value is 0.96 ± 0.06 .

We define small $\Delta\eta$ to be $|\Delta\eta| < 0.5$ and large $\Delta\eta$ to be $1.5 < |\Delta\eta| < 2$ (the upper limit is automatically satisfied because of our single-particle acceptance requirement of $|\eta| < 1$). Note that we have defined equal $|\Delta\eta|$ size for the two regions, but the specific $\Delta\eta$ values for the definitions are less important as long as the large- $\Delta\eta$ region contains minimal near-side contribution. Figure 7(a) shows the $\Delta\phi$ correlations at small and large $\Delta\eta$ for the medium multiplicity range, as an example. The $\Delta\eta$

acceptance has already been corrected in those correlations. The small- and large- $\Delta\eta$ correlations are similar in amplitude, suggesting a more or less uniform two-particle distributions in $\Delta\eta$. The correlations are fit with the functional form of two Gaussians atop a constant pedestal, one Gaussian centered at $\Delta\phi = 0$ and the other at $\Delta\phi = \pm\pi$. The fitted pedestal values are approximately equal between them. Figure 7(b) shows the ratio of the correlations between small and large $\Delta\eta$. The ratio is fit with the same functional form as above, and the fitted pedestal value is 0.96 ± 0.06 .

Figure 8 shows the difference between small- and large- $\Delta\eta$ dihadron correlations, with the large- $\Delta\eta$ correlation first multiplied by the fitted pedestal to the ratio in Fig. 7(b). Because of this choice of normalization, the correlation difference is not necessarily zero outside the near-side region. If we normalized the small- and large- $\Delta\eta$ correlations by matching their away side, then the correlation differences would all be averaged at zero outside the near-side region. For the low-multiplicity bin, there is no near-side peak because of the large negative dipole and likely minimal intra-jet correlations. The near-side peak starts to show up in the mid-multiplicity bin, and is predominant for the high-multiplicity bin, suggesting strong contributions from intra-jet correlations. Resonance decay contributions are likely minimal in SS pairs.

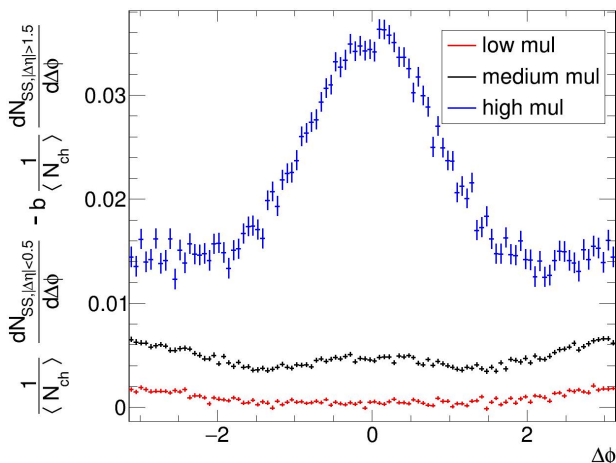


FIG. 8. The differences between small- and large- $\Delta\eta$ dihadron correlations for three multiplicity ranges of $1 \leq N_{\text{ch}} \leq 3$, $4 \leq N_{\text{ch}} \leq 6$, and $15 \leq N_{\text{ch}} \leq 20$, where the large- $\Delta\eta$ correlation is first scaled by a normalization factor. Those correlations for the medium multiplicity range are shown in Fig. 7(a). The normalization factor is taken to be the pedestal value of the corresponding “pedestal + two-Gaussian” fit, such as the one in the lower panel of Fig 7(b); the pedestal values for $1 \leq N_{\text{ch}} \leq 3$ and $15 \leq N_{\text{ch}} \leq 20$ (that are not shown in Fig. 7) are 0.95 ± 0.01 and 0.96 ± 0.07 , respectively.

E. Large $\Delta\eta$ dihadron azimuthal correlations

Large- $\Delta\eta$ is not much contaminated by intra-jet correlations, so it is cleaner to extract flow anisotropies, although dijet correlations are still present on the away side. Figure 9 depicts

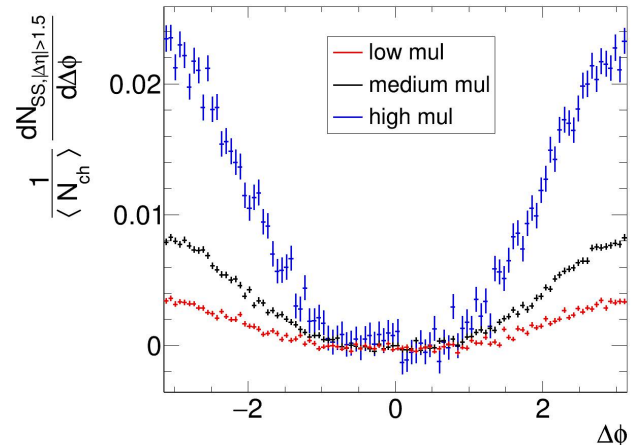


FIG. 9. The SS per-trigger dihadron $\Delta\phi$ correlations at large $\Delta\eta$ ($1.5 < |\Delta\eta| < 2$) in non-diffractive $p+p$ collisions simulated by Pythia 8.303, for three multiplicity ranges $1 \leq N_{\text{ch}} \leq 3$ (low mult.), $4 \leq N_{\text{ch}} \leq 6$ (medium mult.), $15 \leq N_{\text{ch}} \leq 20$ (high mult.). Each distribution is subtracted by the constant pedestal from the “pedestal + Gaussian” fit, like in Fig. 7 for the medium-multiplicity range. The subtracted pedestals are 0.035 ± 0.010 , 0.07 ± 0.0001 , and 0.342 ± 0.001 for the three multiplicity ranges, respectively.

the large- $\Delta\eta$ per-trigger dihadron correlations for the three selected multiplicity bins. For display purpose, the correlations are chopped off a constant pedestal so the near-side region is zero for all three multiplicity ranges. The pedestal is obtained from a “pedestal + Gaussian” fit where the Gaussian describes the away-side correlation about $\Delta\phi = \pm\pi$.

The correlation shapes are similar, with a prominent away-side peak and minimal near-side correlations. The away-side peak is primarily of a negative dipole shape ($-\cos\Delta\phi$); this is in line with the expectation from global momentum conservation [47] and with the expectation that back-to-back dijet correlations at low p_{\perp} are also primarily of a negative dipole shape. The away-side peak amplitude increases with the event multiplicity. This seems to suggest that the back-to-back dijet contribution increases with the event multiplicity, as global momentum conservation should not depend on multiplicity. This is likely due to multiplicity bias—when high-multiplicity is demanded, one is likely selecting events with relatively stronger jet contributions [50–52].

F. Model fits

With the understanding that the SS correlations are composed of intra-jet and dijet correlations atop an underlying event with possible harmonic oscillations, we proceed to fit the mixed-event acceptance corrected ($\Delta\eta, \Delta\phi$) correlations. We use the following fit function:

$$\frac{d^2 N}{d\Delta\eta d\Delta\phi} = A e^{-\frac{(\Delta\eta)^2}{2\sigma_\eta^2}} \left(e^{-\frac{(\Delta\phi)^2}{2\sigma_\phi^2}} + e^{-\frac{(\Delta\phi+2\pi)^2}{2\sigma_\phi^2}} + e^{-\frac{(\Delta\phi-2\pi)^2}{2\sigma_\phi^2}} \right) + A_{\text{RG}} e^{-\frac{(\Delta\eta)^2}{2\sigma_{\text{RG}}^2}} + \frac{B}{2 - |\Delta\eta|} \text{erf}\left(\frac{2 - |\Delta\eta|}{b}\right) + C \left(1 + 2 \sum_{n=1}^4 V_n \cos(n\Delta\phi) \right). \quad (5)$$

The first term on the r.h.s. of Eq. (5) describes the near-side 2D Gaussian in $(\Delta\eta, \Delta\phi)$; the repeated $\Delta\phi$ -Gaussian at $\pm 2\pi$ ensures azimuthal periodicity with those beyond 2π safely neglected. The second term describes the $\Delta\phi$ ridge that is present as a Gaussian at $\Delta\eta = 0$; such a ridge could be the result of beam jet fragmentation aforementioned [53]. The third term attempts to describe a feature present in the correlation functions that bends up towards large $|\Delta\eta|$, which can be attributed to back-to-back emission of particles in both η and ϕ due to, e.g., local momentum conservation; allowing $\eta_1 + \eta_2$ to fluctuate about 0 in Gaussian and integrating it within the acceptance boundaries of $|\eta| < 1$ lead to the marginal distribution of an error function in $\Delta\eta$. The fourth term is the underlying event contribution with possible harmonic oscillations; we keep only the first four harmonics in the fit, where the V_n ($n = 1, 2, 3, 4$) quantify their amplitudes. Note that these harmonic anisotropy amplitudes are with respect to the underlying event multiplicity quantified by the baseline parameter C , excluding contributions from the nonflow (intra-jet and dijet) particles.

We fit the $(\Delta\eta, \Delta\phi)$ SS correlation in each multiplicity bin by Eq. (5). Figure 10 shows, as an example, the fit result for the $7 \leq N_{\text{ch}} \leq 10$ multiplicity bin of the non-diffractive events. The χ^2/NDF values are 1.24, 1.54, 1.12, 1.06, and 0.99 for the multiplicity bins of 1–3, 4–6, 7–10, 11–14, and 15–20 of the non-diffractive events, respectively. For diffractive events, the χ^2/NDF values are 1.78, 1.80, 1.08, 1.01 for the multiplicity bins of 1–3, 4–6, 7–10, and 11–14, respectively. The number of degrees of freedom (NDF) is 3988 for all correlation functions. We note that the χ^2/NDF values are not optimal, suggesting that the fit function of Eq. (5) is not ideal. Nevertheless, the fitted V_n parameters may still give a reasonable description of the underlying modulation.

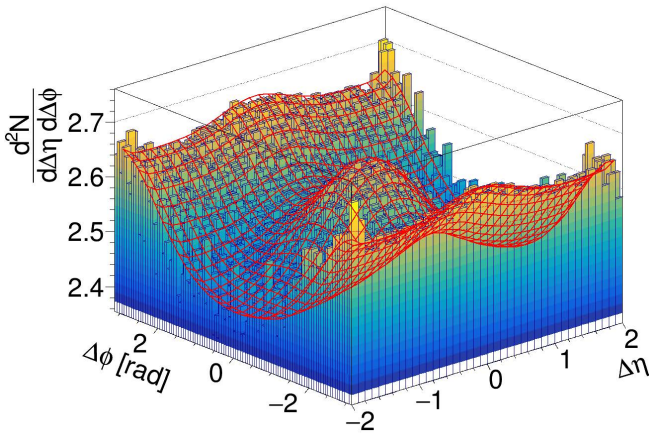


FIG. 10. An example of the 2D model fit by Eq. (5) to the SS pair correlations for the multiplicity range $11 \leq N_{\text{ch}} \leq 14$.

IV. ANISOTROPY RESULTS AND DISCUSSIONS

We are most interested in the V_n parameters. There are multiple ways to obtain V_n , whose physical interpretation depends on the way it is obtained [8]. It can be obtained from the two-particle cumulant by the Fourier coefficient of Eq. (3) as well as by the fitting method of Eq. (5). Figure 11 shows the V_2 obtained by various ways from the SS pair correlations for a selected multiplicity bin of diffractive events and two multiplicity bins of non-diffractive events: the leftmost data point is the Fourier coefficient of SS correlations within $|\Delta\eta| < 0.5$, which gives a large value because of nonflow contribution from the near-side peak; the second leftmost data point is that without any $\Delta\eta$ cut; the third point is that with $|\Delta\eta| > 1.0$ and the fourth one with $|\Delta\eta| > 1.5$, both of which give a significantly reduced value because of the exclusion of the main part of nonflow at small $|\Delta\eta|$; the rightmost data point is the V_2 obtained from the 2D fit, which is the smallest for the results shown, suggesting a large removal of nonflow effects.

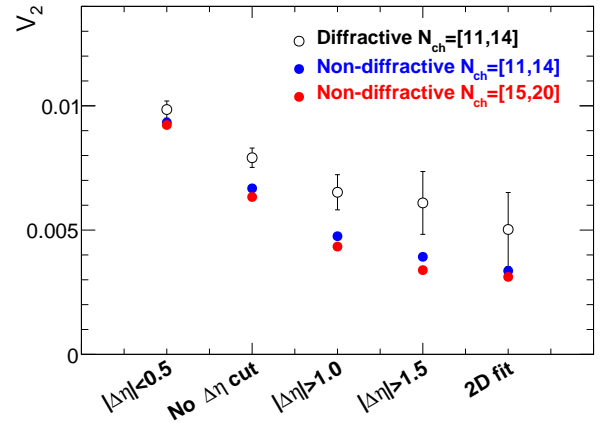


FIG. 11. The V_2 values obtained from SS correlation functions by various methods. Shown are the results for diffractive events of one multiplicity bin and non-diffractive events of two multiplicity bins. The rightmost set of data points are from 2D fits. The rest are Fourier coefficients of correlation functions with various $\Delta\eta$ cuts.

Figure 12 shows V_1 , V_2 , and V_3 values obtained from the Fourier coefficients of the SS correlations at $|\Delta\eta| > 1.5$ (such as the one in Fig. 7(a)) and from the 2D fit to the SS $(\Delta\eta, \Delta\phi)$ correlations. These two methods should have the smallest nonflow contamination. The values are plotted as functions of N_{ch} for both non-diffractive (open black points) and diffractive events (filled red points). It can be appreciated from Fig. 12(a) that the negative dipole V_1 amplitude decreases with increasing multiplicity. However, the multiplicity dependence is not $1/N_{\text{ch}}$, which would be characteristic of global momentum conservation [47]. Thus, the results suggest that the V_1 com-

ponent in those $p + p$ interactions is not of the nature of global momentum conservation. It is interesting to note that the V_1 amplitude is larger in diffractive events than in non-diffractive events at similar multiplicities. The V_1 amplitude from the 2D fit method is generally larger than the Fourier coefficient magnitude from the large- $\Delta\eta$ correlations.

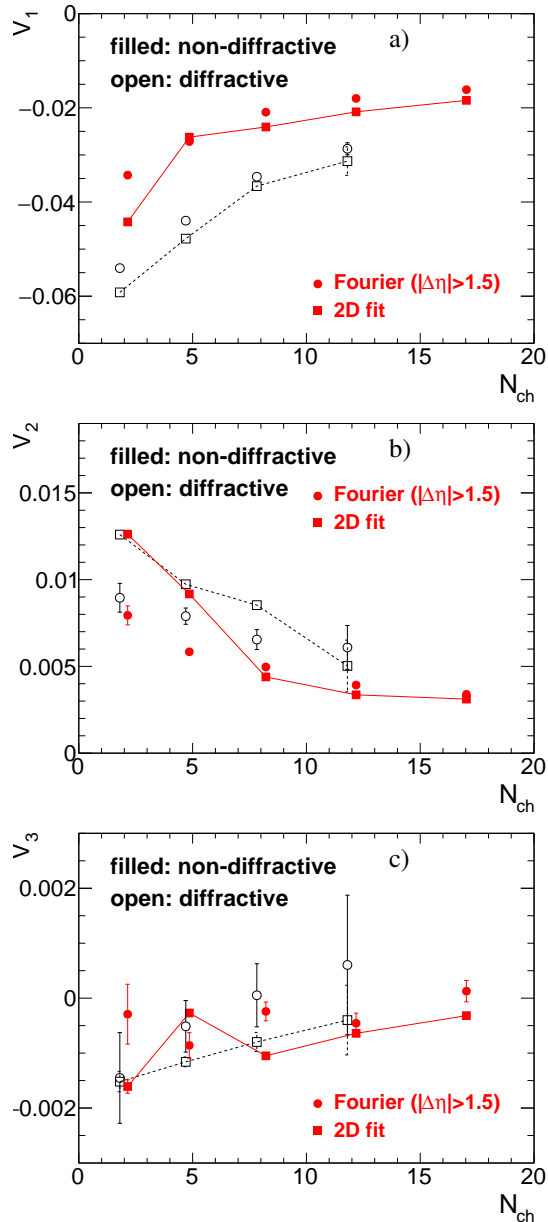


FIG. 12. The V_n parameters obtained from the 2D fit (circles, connected by lines), together with the Fourier coefficients calculated from the SS correlations at $1.5 < |\Delta\eta| < 2$ (squares). Results are shown for diffractive (open black points) and non-diffractive (filled red points) events as functions of multiplicity.

The V_2 coefficient shown in Fig. 12(b) is positive and exhibits a decreasing trend with multiplicity. The trends may be suggestive of nonflow, which would be inversely proportional to multiplicity (e.g., nonflow contribution from the near-side

peak). It is possible that the 2D fits are not adequate to separate the correlations into flow and nonflow in those $p + p$ interactions, such that the fitted harmonics still reflect some nonflow characteristics. It is interesting to notice that the 2D fit V_2 values in the two lowest multiplicity bins of non-diffractive events are higher than the Fourier coefficients calculated at large $|\Delta\eta| > 1.5$, while they are close to each other for the three higher multiplicity bins. This may reflect the difficulty in fitting the nonflow components in those low multiplicity events. The reason for this difficulty might be due to the fact that the near-side peak does not have a large presence and is barely noticeable for the two low multiplicity bins. It is also noteworthy that the fitted V_1 and V_2 parameters are anti-correlated, and this may play a role in the lowest multiplicity bin of the non-diffractive events. It may be at play for the diffractive events, where the three low multiplicity bins reveal larger fit V_2 and more negative fit V_1 than the Fourier counterparts.

Finally, the V_3 coefficient shown in Fig. 12(c) is close to zero with large uncertainties. The overall magnitude may be negative, suggestive of influence of away-side peak.

One way to mitigate nonflow contributions is to subtract correlations in low-multiplicity events from those in high-multiplicity events [8]. This is possible under the assumption that the nonflow correlation shape does not change with multiplicity and the abundance of the nonflow correlation sources is proportional to multiplicity [8]. The latter also assumes, implicitly, that there are no biases to nonflow correlations from selection of events according to the event multiplicity. Under these assumptions, the “flow” harmonics in high-multiplicity events would be

$$V_n^{\text{sub}} = V_n^{\text{high}} - \frac{N^{\text{low}}}{N^{\text{high}}} V_n^{\text{low}}, \quad (6)$$

where the superscript ‘high’ and ‘low’ denote those quantities in high- and low-multiplicity events, respectively. Figure 13 shows the V_2^{sub} as functions of multiplicity for non-diffractive events. The results are shown for two cases, one uses SS correlations without any $\Delta\eta$ cut, and the other uses those with $|\Delta\eta| > 1.5$. The results differ, and the interpretation can be either (i) that they may reflect collective flow—which can be possible in $p + p$ interactions because of multi-parton interactions or color reconnection—and there is a strong $\Delta\eta$ decorrelation effect, or (ii) that they may not reflect collective flow—which is naively expected to be $\Delta\eta$ independent due to its origin in early dynamics—but nonflow as nonflow is not independent of multiplicity or there are strong multiplicity biases in event selection. For comparison, the 2D fit V_2 values in the three high multiplicity bins are also plotted in Figure 13; those for the lower multiplicity bins are significantly higher as seen from Fig. 12. No obvious systematics are apparent from the comparison.

The V_2^{sub} results shown in Fig. 13 from the various methods suggest the single-particle azimuthal anisotropy $v_2 = \sqrt{V_2}$ of the order of 5–7%. This is comparable to experimental findings at the LHC [22–24], despite of the lower RHIC energy used in our simulation. This is especially the case for the V_2^{sub} results extracted from correlations in the large- $\Delta\eta$ region of $|\Delta\eta| > 1.5$, the approximate region used in LHC

experiments. It would be interesting to further investigate the possible anisotropic flows in Pythia simulations of $p + p$ interactions at LHC energies [40].

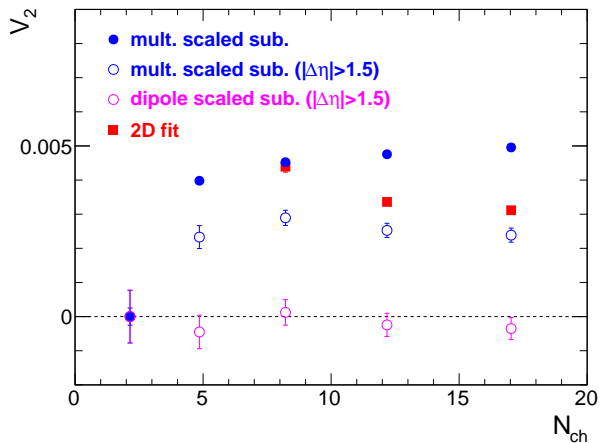


FIG. 13. Low-multiplicity subtracted V_2 values as functions of multiplicity. Inverse multiplicity scaled subtraction (blue points) is shown for no $\Delta\eta$ cut and $|\Delta\eta| > 1.5$. Dipole-scaled subtraction (pink points) is shown for $|\Delta\eta| > 1.5$. Also shown are V_2 values from 2D fit (red squares). Results are obtained from SS correlation functions of non-diffractive events.

Another recipe for nonflow subtraction is to assume that the negative V_1 dipole is all nonflow and the nonflow correlation shape does not change with multiplicity, i.e., the nonflow V_n ($n > 1$) is proportional to V_1 . This would lead to

$$V_n^{\text{sub}} = V_n^{\text{high}} - \frac{V_1^{\text{high}}}{V_1^{\text{low}}} V_n^{\text{low}}. \quad (7)$$

The V_2^{sub} values obtained from this dipole-scaled subtraction are shown by the pink points in Fig. 13 for SS correlations at $|\Delta\eta| > 1.5$. They are all consistent with zero, implying that the V_1 and V_2 harmonics of the large- $\Delta\eta$ SS correlations scale with each other, which is indeed the case by comparing Fig. 12(a) and Fig. 12(b).

V. SUMMARY

Azimuthal anisotropies have been observed in high-energy small-system (proton-proton and proton/deuteron/ ^3He -nucleus) collisions, similar to those measured in relativistic heavy ion collisions. This raises an intriguing possibility of collective flow behavior and the formation of a quark-gluon plasma droplet in those small-system collisions and has

aroused intense interests. Because of severe contamination of nonflow (genuine few-body) correlations in those small systems, analysis and interpretation of the two-particle azimuthal cumulant anisotropies are challenging. Several nonflow mitigation methods are available with various assumptions and degrees of validity. At least three interpretations are possible: (i) the measured anisotropies are part of nonflow correlations that differ from low- to high-multiplicity events; (ii) the measured anisotropies are a result of multi-parton interactions and color connections which are different from hydrodynamic-like interactions in the final state of heavy ion collisions; and (iii) there is an appreciable contribution from hydrodynamic-like final-state interactions, thus collective flow, in those small-system collisions.

To shed further lights, we have studied two-particle angular correlations in pseudorapidity and azimuthal differences in simulated $p + p$ interactions by the Pythia 8.303 event generator. The model includes multi-parton interactions and color reconnection, but no final-state interactions or hydrodynamic expansion. We present our study in a pedagogical way and report azimuthal anisotropies extracted by several methods. These methods have different assumptions and sensitivities to nonflow correlations and, as such, our results represent a fair range in analysis method dependency and degree of validity. We observe finite azimuthal anisotropies from several, but not all, of the employed methods. The results are qualitatively, and in some cases semi-quantitatively, similar to those observed in experimental data. Our study, therefore, provides an important benchmark helping improve data analysis and interpret experimental findings.

There are a number of ways to build up on and further enhance our study. One is to turn off multi-parton interactions and color reconnection to examine the effects on the final azimuthal anisotropies. Another is to simulate $p + p$ interactions at the higher LHC energies and expand to proton-nucleus and nucleus-nucleus collisions by the same Pythia model, and investigate the systematics of the azimuthal anisotropies on system size and collision energy. A thorough comparison of experimental data to Pythia simulations with variations in physics processes, at the level of both the raw correlation functions and the extracted azimuthal anisotropies, should be performed. Some of those studies are already available in the literature, but a systematic study would be invaluable.

ACKNOWLEDGMENT

MST acknowledges support from the Purdue-Colombia Exchange and Partnership Program. This work is supported in part by the U.S. Department of Energy (Grant No. DE-SC0012910).

[1] J.-Y. Ollitrault, Anisotropy as a signature of transverse collective flow, *Phys.Rev.* **D46**, 229 (1992).

[2] U. Heinz and R. Snellings, Collective flow and viscosity in relativistic heavy-ion collisions, *Ann.Rev.Nucl.Part.Sci.* **63**, 123 (2013), arXiv:1301.2826 [nucl-th].

- [3] S. Voloshin and Y. Zhang, Flow study in relativistic nuclear collisions by Fourier expansion of Azimuthal particle distributions, *Z.Phys.* **C70**, 665 (1996), arXiv:hep-ph/9407282 [hep-ph].
- [4] A. M. Poskanzer and S. Voloshin, Methods for analyzing anisotropic flow in relativistic nuclear collisions, *Phys.Rev.* **C58**, 1671 (1998), arXiv:nucl-ex/9805001 [nucl-ex].
- [5] N. Borghini, P. M. Dinh, and J.-Y. Ollitrault, Are flow measurements at SPS reliable?, *Phys.Rev.* **C62**, 034902 (2000), arXiv:nucl-th/0004026 [nucl-th].
- [6] Q. Wang and F. Wang, Non-flow correlations in a cluster model, *Phys.Rev.* **C81**, 064905 (2010), arXiv:0812.1176 [nucl-ex].
- [7] J.-Y. Ollitrault, A. M. Poskanzer, and S. A. Voloshin, Effect of flow fluctuations and nonflow on elliptic flow methods, *Phys.Rev.* **C80**, 014904 (2009), arXiv:0904.2315 [nucl-ex].
- [8] Y. Feng and F. Wang, Review of nonflow estimation methods and uncertainties in relativistic heavy-ion collisions (2024), arXiv:2407.12731 [nucl-ex].
- [9] V. Khachatryan *et al.* (CMS Collaboration), Observation of Long-Range Near-Side Angular Correlations in Proton-Proton Collisions at the LHC, *JHEP* **1009**, 091, arXiv:1009.4122 [hep-ex].
- [10] S. Chatrchyan *et al.* (CMS Collaboration), Observation of long-range near-side angular correlations in proton-lead collisions at the LHC, *Phys.Lett.* **B718**, 795 (2013), arXiv:1210.5482 [nucl-ex].
- [11] G. Aad *et al.* (ATLAS Collaboration), Observation of Associated Near-side and Away-side Long-range Correlations in $\sqrt{s_{NN}}=5.02$ TeV Proton-lead Collisions with the ATLAS Detector, *Phys.Rev.Lett.* **110**, 182302 (2013), arXiv:1212.5198 [hep-ex].
- [12] B. Abelev *et al.* (ALICE Collaboration), Long-range angular correlations on the near and away side in p -Pb collisions at $\sqrt{s_{NN}}=5.02$ TeV, *Phys.Lett.* **B719**, 29 (2013), arXiv:1212.2001.
- [13] B. B. Abelev *et al.* (ALICE Collaboration), Long-range angular correlations of π , K and p in p -Pb collisions at $\sqrt{s_{NN}}=5.02$ TeV, *Phys.Lett.* **B726**, 164 (2013), arXiv:1307.3237 [nucl-ex].
- [14] L. Adamczyk *et al.* (STAR Collaboration), Long-range pseudorapidity dihadron correlations in d +Au collisions at $\sqrt{s_{NN}}=200$ GeV, *Phys.Lett.* **B747**, 265 (2015), arXiv:1502.07652 [nucl-ex].
- [15] M. Aaboud *et al.* (ATLAS), Measurements of long-range azimuthal anisotropies and associated Fourier coefficients for pp collisions at $\sqrt{s}=5.02$ and 13 TeV and p +Pb collisions at $\sqrt{s_{NN}}=5.02$ TeV with the ATLAS detector, *Phys. Rev. C* **96**, 024908 (2017), arXiv:1609.06213 [nucl-ex].
- [16] C. Aidala *et al.* (PHENIX), Measurements of Multiparticle Correlations in d +Au Collisions at 200, 62.4, 39, and 19.6 GeV and p +Au Collisions at 200 GeV and Implications for Collective Behavior, *Phys. Rev. Lett.* **120**, 062302 (2018), arXiv:1707.06108 [nucl-ex].
- [17] C. Aidala *et al.* (PHENIX), Creation of quark-gluon plasma droplets with three distinct geometries, *Nature Phys.* **15**, 214 (2019), arXiv:1805.02973 [nucl-ex].
- [18] U. A. Acharya *et al.* (PHENIX), Kinematic dependence of azimuthal anisotropies in $p+Au$, $d+Au$, and ${}^3\text{He}+Au$ at $\sqrt{s_{NN}}=200$ GeV, *Phys. Rev. C* **105**, 024901 (2022), arXiv:2107.06634 [hep-ex].
- [19] M. I. Abdulhamid *et al.* (STAR), Measurements of the Elliptic and Triangular Azimuthal Anisotropies in Central He3+Au, d+Au and p+Au Collisions at $s_{NN}=200$ GeV, *Phys. Rev. Lett.* **130**, 242301 (2023), arXiv:2210.11352 [nucl-ex].
- [20] S. Acharya *et al.* (ALICE), Emergence of Long-Range Angular Correlations in Low-Multiplicity Proton-Proton Collisions, *Phys. Rev. Lett.* **132**, 172302 (2024), arXiv:2311.14357 [nucl-ex].
- [21] Measurement of flow coefficients in high-multiplicity p +Au, d +Au and ${}^3\text{He}+Au$ collisions at $\sqrt{s_{NN}}=200$ GeV (2023), arXiv:2312.07464 [nucl-ex].
- [22] S. Chatrchyan *et al.* (CMS), Multiplicity and Transverse Momentum Dependence of Two- and Four-Particle Correlations in pPb and PbPb Collisions, *Phys. Lett. B* **724**, 213 (2013), arXiv:1305.0609 [nucl-ex].
- [23] G. Aad *et al.* (ATLAS Collaboration), Measurement with the ATLAS detector of multi-particle azimuthal correlations in p +Pb collisions at $\sqrt{s_{NN}}=5.02$ TeV, *Phys.Lett.* **B725**, 60 (2013), arXiv:1303.2084 [hep-ex].
- [24] S. Acharya *et al.* (ALICE), Investigations of Anisotropic Flow Using Multiparticle Azimuthal Correlations in pp, p-Pb, Xe-Xe, and Pb-Pb Collisions at the LHC, *Phys. Rev. Lett.* **123**, 142301 (2019), arXiv:1903.01790 [nucl-ex].
- [25] W. Li, Observation of a 'Ridge' correlation structure in high multiplicity proton-proton collisions: A brief review, *Mod.Phys.Lett.* **A27**, 1230018 (2012), arXiv:1206.0148 [nucl-ex].
- [26] J. L. Nagle and W. A. Zajc, Small System Collectivity in Relativistic Hadronic and Nuclear Collisions, *Ann. Rev. Nucl. Part. Sci.* **68**, 211 (2018), arXiv:1801.03477 [nucl-ex].
- [27] L. He, T. Edmonds, Z.-W. Lin, F. Liu, D. Molnar, and F. Wang, Anisotropic parton escape is the dominant source of azimuthal anisotropy in transport models, *Phys. Lett.* **B753**, 506 (2016), arXiv:1502.05572 [nucl-th].
- [28] P. Romatschke, Relativistic Fluid Dynamics Far From Local Equilibrium, *Phys. Rev. Lett.* **120**, 012301 (2018), arXiv:1704.08699 [hep-th].
- [29] A. Kurkela and A. Mazeliauskas, Chemical equilibration in weakly coupled QCD, *Phys. Rev.* **D99**, 054018 (2019), arXiv:1811.03068 [hep-ph].
- [30] A. Kurkela, A. Mazeliauskas, and R. Törnkvist, Collective flow in single-hit QCD kinetic theory, *JHEP* **11**, 216, arXiv:2104.08179 [hep-ph].
- [31] D. d'Enterria, G. K. Eyyubova, V. L. Korotkikh, I. P. Lokhtin, S. V. Petrushanko, L. I. Sarycheva, and A. M. Snigirev, Estimates of hadron azimuthal anisotropy from multiparton interactions in proton-proton collisions at $\sqrt{s}=14$ TeV, *Eur. Phys. J.* **C66**, 173 (2010), arXiv:0910.3029 [hep-ph].
- [32] A. Ortiz Velasquez, P. Christiansen, E. Cuautle Flores, I. Maldonado Cervantes, and G. Paić, Color Reconnection and Flow-like Patterns in pp Collisions, *Phys. Rev. Lett.* **111**, 042001 (2013), arXiv:1303.6326 [hep-ph].
- [33] C. Bierlich, G. Gustafson, and L. Lönnblad, Collectivity without plasma in hadronic collisions, *Phys. Lett.* **B779**, 58 (2018), arXiv:1710.09725 [hep-ph].
- [34] T. Sjöstrand, Collective Effects: the viewpoint of HEP MC codes (2018) arXiv:1808.03117 [hep-ph].
- [35] T. Sjöstrand, High-energy physics event generation with PYTHIA 5.7 and JETSET 7.4, *Comput. Phys. Commun.* **82**, 74 (1994).
- [36] T. Sjöstrand, S. Ask, J. R. Christiansen, R. Corke, N. Desai, P. Ilten, S. Mrenna, S. Prestel, C. O. Rasmussen, and P. Z. Skands, An introduction to PYTHIA 8.2, *Comput. Phys. Commun.* **191**, 159 (2015), arXiv:1410.3012 [hep-ph].
- [37] T. Sjöstrand, The PYTHIA Event Generator: Past, Present and Future, *Comput. Phys. Commun.* **246**, 106910 (2020), arXiv:1907.09874 [hep-ph].
- [38] C. Bierlich *et al.*, A comprehensive guide to the physics and usage of PYTHIA 8.3, *SciPost Phys. Codeb.* **2022**, 8 (2022), arXiv:2203.11601 [hep-ph].
- [39] T. Sjöstrand, The Development of MPI Modeling in Pythia, *Adv. Ser. Direct. High Energy Phys.* **29**, 191 (2018),

- arXiv:1706.02166 [hep-ph].
- [40] C. Bierlich, G. Gustafson, L. Lönnblad, and H. Shah, The Angantyr model for Heavy-Ion Collisions in PYTHIA8, *JHEP* **10**, 134, arXiv:1806.10820 [hep-ph].
- [41] S. H. Lim, Q. Hu, R. Belmont, K. K. Hill, J. L. Nagle, and D. V. Perepelitsa, Examination of flow and nonflow factorization methods in small collision systems, *Phys. Rev. C* **100**, 024908 (2019), arXiv:1902.11290 [nucl-th].
- [42] M. I. Abdulhamid, A. M. Hamed, E. A. Osama, M. Rateb, N. K. Sadoun, and F. H. Sawy, Benchmarking the Non-flow Contributions to the Elliptic Flow Parameter (v_2) in Proton-Proton Collisions (2024), arXiv:2405.13981 [hep-ph].
- [43] T. Sjostrand, S. Mrenna, and P. Z. Skands, PYTHIA 6.4 Physics and Manual, *JHEP* **05**, 026, arXiv:hep-ph/0603175.
- [44] K. Ackermann *et al.* (STAR Collaboration), STAR detector overview, *Nucl.Instrum.Meth.* **A499**, 624 (2003).
- [45] J. Alme *et al.*, The ALICE TPC, a large 3-dimensional tracking device with fast readout for ultra-high multiplicity events, *Nucl. Instrum. Meth. A* **622**, 316 (2010), arXiv:1001.1950 [physics.ins-det].
- [46] F. Wang, Novel Phenomena in Particle Correlations in Relativistic Heavy-Ion Collisions, *Prog. Part. Nucl. Phys.* **74**, 35 (2014), arXiv:1311.4444 [nucl-ex].
- [47] N. Borghini, Momentum conservation and correlation analyses in heavy-ion collisions at ultrarelativistic energies, *Phys. Rev.* **C75**, 021904 (2007), arXiv:nucl-th/0612093 [nucl-th].
- [48] P. Jacobs and X.-N. Wang, Matter in extremis: Ultrarelativistic nuclear collisions at RHIC, *Prog.Part.Nucl.Phys.* **54**, 443 (2005), arXiv:hep-ph/0405125 [hep-ph].
- [49] J. Adams *et al.* (STAR Collaboration), Distributions of charged hadrons associated with high transverse momentum particles in pp and Au + Au collisions at $\sqrt{s_{NN}} = 200$ -GeV, *Phys.Rev.Lett.* **95**, 152301 (2005), arXiv:nucl-ex/0501016 [nucl-ex].
- [50] A. Adare *et al.* (PHENIX), Centrality categorization for $R_{p(d)+A}$ in high-energy collisions, *Phys. Rev. C* **90**, 034902 (2014), arXiv:1310.4793 [nucl-ex].
- [51] L. Adamczyk *et al.* (STAR Collaboration), Effect of event selection on jetlike correlation measurement in $d+Au$ collisions at $\sqrt{s_{NN}} = 200$ GeV, *Phys. Lett.* **B743**, 333 (2015), arXiv:1412.8437 [nucl-ex].
- [52] S. Acharya *et al.* (ALICE), Analysis of the apparent nuclear modification in peripheral Pb–Pb collisions at 5.02 TeV, *Phys. Lett. B* **793**, 420 (2019), arXiv:1805.05212 [nucl-ex].
- [53] B. Andersson, G. Gustafson, G. Ingelman, and T. Sjostrand, Parton Fragmentation and String Dynamics, *Phys. Rept.* **97**, 31 (1983).